2005 7th International Conference on Information Fusion (FUSION)

Color Segmentation Using an Eigen Color Representation

Alaa E. Abdel-Hakim and Aly A. Farag
Computer Vision and Image Processing Laboratory (CVIP Lab.)
University of Louisville, Louisville/40292, KY
USA
{alaa,farag}@cvip.uofl.edu
http://www.cvip.uofl.edu

Abstract— **In real images, color segmentation is a challenging problem because of natural variations in light and shadows. Most existing color models have limitations in distinctive representation of colors in real scenes. Color segmentation approaches are highly dependent on the robustness of the used color model to these variations. In this paper, we present a novel color representation for color segmentation. The proposed model is a fusion of classical color representations. It is calculated using a closed form linear transformation from a high dimensional classical feature space to a lower dimensional new space. We prove the high performance of the proposed model in terms of robustness to natural variations and distinction between different colors, when compared with classical color models. Through color segmentation of real images, we provide a quantitative and qualitative comparison between the proposed model and classical models. The experimental results support the potential of the proposed model.[1].**

I. Introduction

Color representation is a cornerstone in many computer vision and image processing applications. Several color spaces were developed for graphics and digital image processing [1],e.g. Red, Green, Blue (RGB), Hue, Saturation. Intensity (HSI), and XYZ. The performance of any color-dependent system is highly influenced by the color model it uses. The quality of a color model is determined by the distinction between different colors in the model, and the robustness of any single color representation against the natural variations in real scenes, such as light changes and shadows. These two criteria seem to be conflicting, which represents a real challenge to any color representation scheme.

Several recent researches in the literature have tried to compromise between these two constraints. For example, color lines were presented in [2] as an image color representation. Color lines are constructed for each image, i.e. every single image has its own color representation. So, the main limitation in the color lines is the dependence of the model on the image it represents. In [3], [4], soccer players are classified, according to their color information, using supervised learning techniques. In that approach, the dominant features in different color spaces are selected to construct a reduced "*Hybrid Color Space, HCS*". However, there are some limitations in the HCS. For example, to select the dominant features, an objective function is iteratively optimized by evaluating possible combinations of the candidate models' primaries. Practically, it is almost impossible to test all possible combinations, since they have a combinatory number equal to the factorial of the total number of the candidate primaries. Therefore, HCS is constructed by searching for an acceptable combination of features which approximately optimize the objective function. Also, the primaries of HCS are exactly similar to the selected primaries from the candidate space. This means that more candidate models are recommended for getting a better representation. Unfortunately, more candidate models mean bigger search space and hence larger approximation in the final solution.

In this paper, we present "*Eigen Color Basis*" (*ECB*) as a novel color representation. ECB is calculated using a closed form linear transformation from a high dimensional classical feature space to the lower dimensional ECB space. The transformation used to construct the ECB is optimal and guarantees better performance than the existing classical models. Also, it is general enough to be applied to any color-dependent application. The color segmentation results support the good quality of ECB, in terms of robustness and distinction, when compared to classical models.

The rest of the paper goes as follows: in section two, we present an overview of the most known color models. We explore the advantages and drawbacks for each one. In section three, we explain the proposed ECB model. Also, we discuss the quantitative evaluation criteria which we used to evaluate the performance of the proposed model versus the classical ones. In section four, we give an overview of three of the most known pixel-based color classification approaches. In section five, we show the quantitative evaluation results and sample results for segmentation based on ECB and the other models, for qualitative comparison

II. Classical Color Models

Most display and color acquisition devices, such as digital cameras and scanners, have their input or output signals in the RGB format. This is why RGB space is widely used in the applications of image processing. However, RGB representation

[1]This work is supported by US Army under grant DABT60-02-P-0063

has several drawbacks that decrease the performance of the systems which depend on it. RGB space is not uniform, i.e. the relative distances between colors do not reflect the perceptual differences. For example, in the color gamut of RGB space the distance between blue=(0,0,1) and magenta=(1,0,1) equals the distance between magenta and white=(1,1,1). However, the human vision system considers the perceptual distance between blue and magenta less than the distance between white and magenta. Another important disadvantage of the RGB space is the high influence of incident light and specularity on the values of color primaries. In other words, a particular surface has RGB values less than those of the same surface with brighter shinning light. To decrease the dependence on illumination intensity, the normalized RGB (NRGB), or the chromaticity coordinates, was developed [1], as shown in Eq.(1).

$$r = \frac{R}{R+G+B}, g = \frac{G}{R+G+B}, b = \frac{B}{R+G+B} \quad (1)$$

For the human brain, the color values in the RGB model are hard to interpret as a perceived color. Therefore, HSI space has been developed as a closer representation to the human perception system, which can easily interpret the primaries of this space. In HSI space, the dominant wavelength of color is represented by the hue component. The purity of color is represented by the saturation component. Finally, the darkness or the lightness of color is determined by the intensity component.Eq.(2) shows the transformation between RGB and HSI spaces [5]. Some other alternative color models of HSI, such as HSV and HLS [6], [7], [8] are used in computer graphics and other vision applications.

$$\begin{aligned} I &= \tfrac{1}{3}(R+G+B) \quad (2)\\ S &= 1 - \tfrac{3}{R+G+B}[min(R,G,B)]\\ H &= \begin{cases} \theta & B \le G \\ 360-\theta & B > G \end{cases}\\ where \theta &= \cos^{-1}\{\tfrac{0.5[(R-G)+(R-B)]}{\sqrt{(R-G)^2+(R-B)(G-B)}}\} \end{aligned}$$

Although the HSI space is more suitable for the application of color images, especially color segmentation, there are still some problems with it. Specifically, there are non-avoidable singularities in the transformation from RGB to HSI, as shown in Eq.(2). HSI values are very sensitive to any change in the RGB values near those singularities. Also, there is a similar problem to that of RGB space, which is the non-uniform correspondence between the distances in the model and human color perception. This is because the uniform change in the SI plane does not correspond to a uniform change in human perception. For example, the change in the perceived color due to a saturation variation in low intensity is less than that at high intensity.

XYZ color space was developed by *Commission Internationale De L'eclairage (CIE)* in 1931 [9]. The color basis in the XYZ is not similar to that of RGB space. The R primary in RGB corresponds to the amount of the physical reflected light in the red band. But in XYZ space, every primary does not correspond to a specific physical light. Instead, the colors are represented by luminance in one dimension and chromaticity in the other two dimensions. This design of the XYZ basis guarantees that there is no negative tristimulus for any color in the visible spectrum.

The YUV model is one of the XYZ representations. It has been developed for display applications. The YUV model stores the color in a way similar to the way which the human brain uses for color perception. The YUV model consists of the luma (Y), which is similar to the intensity component in HSI space. The color information is represented by two components U (or C_b) and V (or C_r). U is the blue/yellow measure such that positive values mean bluish and negative values mean yellowish. Similarly, V is the red/green measure such that positive values mean reddish and negative values mean greenish. This representation comes from the fact that the human brain thinks about red and blue as the opposite components to green and yellow, respectively. Another alternative of YUV is the YIQ which is used in the NTSC TV standard. In YIQ, the Y component is the same as that of YUV, while IQ is an axis pair rotated 33^o from the UV-axis pair.

Ohta, Kanade, and Sakai [10] have selected a set of "effective" color features after analyzing 100 different color features which have been used in segmenting eight kinds of color images. Those selected color features, which we will term "*Ohta*" color model, are calculated linearly from RGB space. So, XYZ, YUV, and Ohta are linear transformations of RGB space. Therefore, they are non-uniform color spaces, i.e. the distance correspondence with the human perception is non-uniform. CIE has recommended CIE-Lab and CIE-Luv as uniform color spaces, as they are non-linear transformation of RGB space [8].

III. Eigen Color Basis

Assume that we have n samples of colored pixels from C color classes ($n \gg C$). The color of each pixel, in a d-dimension color basis, is given by:

$$\mathbf{P} = \begin{bmatrix} c_1 & c_2 & . & . & c_d \end{bmatrix}^t \quad (3)$$

The quality of a color basis is judged by two criteria: "*Robustness*" and "*Distinction*". The robustness of the color representation is an indication of the sensitivity of the color values to illumination and brightness variations. The distinction of a color basis represents how distinct every color is from the other colors modelled by the same basis. The robustness of a color basis is inversely related to the inter-class distance. The "*within-class scatter matrix*", shown in Eq.(4), can be used as a measure for the interclass variation [11].

$$\mathbf{S}_W = \sum_{k=1}^{C} \mathbf{S}_k; \mathbf{S}_k = \sum_{\mathbf{P} \in Z_k} (\mathbf{P} - \mathbf{m}_k)(\mathbf{P} - \mathbf{m}_k)^t \quad (4)$$

where Z_k is the sample subset belonging to color class k and m_k is the mean vector of color class k

The distinction is achieved by maximizing the intra-class distances. The "*between-class scatter matrix*", shown in

Eq.(5), is used to indicate how far the classes are from each other.

$$\mathbf{S}_B = \sum_{k=1}^{C} n_k(\mathbf{m} - \mathbf{m}_k)(\mathbf{m} - \mathbf{m}_k)^t \quad (5)$$

where n_k is the number of samples subset belongs to color class k and m is the total mean vector.

To achieve both of those criteria at the same time, the criterion function of Eq.(6), is to be maximized [11].

$$J = \frac{|\mathbf{S}_B|}{|\mathbf{S}_W|} \quad (6)$$

Our goal is to define a color basis that maximizes this criterion function. Assume that we have M classical color models with a total of K color primaries. An integrated color descriptor ($\mathbf{P}_I$) is built as shown in Eq.(7).

$$\mathbf{P}_I = \begin{bmatrix} \mathbf{P}_1^t & \mathbf{P}_2^t & . & . & \mathbf{P}_K^t \end{bmatrix}^t \quad (7)$$

The color descriptor of the same pixel in ECB is defined as shown in Eq.(8).

$$\tilde{\mathbf{P}} = \begin{bmatrix} \tilde{c}_1 & \tilde{c}_2 & . & . & \tilde{c}_E \end{bmatrix}^t \quad (8)$$

Hence, the dimension of the ECB is $E \leq K$. $\tilde{\mathbf{P}}$ and $\mathbf{P}_I$ are related by the transformation of Eq.(9).

$$\tilde{\mathbf{P}} = \mathbf{W}^t\mathbf{P}_I; \mathbf{W} : K \times E \quad (9)$$

So, the ECB is completely defined, if $\mathbf{W}$ is known. $\mathbf{W}$ should be estimated such that the criterion function of Eq.(6) for ECB ($\tilde{J}$) is maximized.

$$\mathbf{W} = \arg\{\max[\tilde{J}(\mathbf{W})]\} = \arg\{\max[\frac{|\tilde{\mathbf{S}}_B|}{|\tilde{\mathbf{S}}_W|}]\} \quad (10)$$

$$\tilde{\mathbf{S}}_W = \mathbf{W}^t\mathbf{S}_W\mathbf{W} \quad (11a)$$

$$\tilde{\mathbf{S}}_B = \mathbf{W}^t\mathbf{S}_B\mathbf{W} \quad (11b)$$

By substituting Eq.(11) in Eq.(10), $\mathbf{W}$ will be the argument of the generalized Rayliegh quotient, as shown in Eq.(12).

$$\mathbf{W} = \arg\{\max[\tilde{J}(\mathbf{W})]\} = \arg\{\max[\frac{|\mathbf{W}^t\mathbf{S}_B\mathbf{W}|}{|\mathbf{W}^t\mathbf{S}_W\mathbf{W}|}]\} \quad (12)$$

The solution of Eq.(12) is calculated such that the columns of $\mathbf{W}$ are the principle components, i.e. the generalized eigen vectors that correspond to the largest eigen values in Eq.(13) [11].

$$\mathbf{S}_B\mathbf{W}_i = \lambda_i\mathbf{S}_W\mathbf{W}_i \quad (13)$$

If $\mathbf{S}_w$ is nonsingular, then finding $\mathbf{W}$ is straight forward. However, the computation of the inverse of $\mathbf{S}_w$ can be avoided by finding the roots of the characteristic polynomial of Eq.(14). Then, Eq.(15) can be solved for the eigen vectors $\mathbf{w}_i$. There are other methods that deal with the special cases of $\mathbf{S}_w$ such as singular and isotropic cases [11].

$$|\mathbf{S}_B - \lambda_i\mathbf{S}_W| = 0 \quad (14)$$

$$(\mathbf{S}_B - \lambda_i\mathbf{S}_W)\mathbf{w}_i = 0 \quad (15)$$

It is known from principle component analysis that reducing the feature dimension space produces an error or information loss which can be calculated as shown in Eq.(16).

$$Loss(\%) = (1.0 - \frac{\sum_{i=1}^{d} D_i}{\sum_{j=1}^{K} D_j}) \times 100 \quad (16)$$

where D_i is the i^th eigen value, d is dimension of the reduced feature space, and K is the dimension of the full feature space.

At the same time, reducing the dimension of the feature space reduces the interset and the intraset distances, as well. Hence, this reduction may lead to a higher Rayleigh quotient. In this case, a compromise should be done, as discussed in section five.

Besides the generalized Raleigh quotient as a performance description criterion for color models, we use another criterion to evaluate the color segmentation process using different color models. This criterion is the *Specificity-Sensitivity* measure. The specificity is defined as the ratio between the number of the correct classified pixels and the total number of pixels assigned to the same class. The sensitivity is defined as the ratio between the number of correct classified pixels and the actual number of pixels in the same class [12]. We denote the geometric mean of the specificity and sensitivity as the *Specificity-Sensitivity (SS)* measure, while the ratio between the intraset and the interest distances is denoted as the *Robustness-Distinction (RD)* measure.

IV. Color Classification

Color segmentation approaches can be divided into pixel-based approaches, region-based approaches, and color edge approaches [13]. To prove the potential of the proposed model, in this section, we discuss in details statistical pixel-based color classification approaches. In general, the process of color classification in real images can be considered as a composite of two random processes: a high level random process ($\mathbf{G}^h$) that describes the various color regions in the images, and a low level random process ($\mathbf{G}^l$) that describes each particular color dependence in each region [14]. For an image with C color classes and q color levels, the processes $\mathbf{G}^h$ and $\mathbf{G}^l$ are discrete parameter random fields with their state spaces defined as follows:

$$\Xi^h = \{\xi^h : \xi^h \in [1, C]\} \quad (17a)$$

$$\Xi^l = \{\xi^l : \xi^l \in [1, q-1]\} \quad (17b)$$

The high-level process $\mathbf{G}^h$ can be described as follows: consider a lattice $S = \{s = (x, y) : x \in [0, M-1], y \in [0, N-1]\}$; for each pixel $s \in S, g^h(s) = k$ denotes that s belongs to the color class $k \in [1, C]$. The observed image g can now be described as follows: consider a color class k; the color value at pixel $s \in S$ of the observed image g equals that of the color class k, that is, $g(s) = g^{l_k}(s)$ if $g^h(s) = k \forall k \in [1, C]$ and $s \in S$; where $g^{l_k}(.)$ denotes the color value in the color class k.

A possible segmentation criterion can be the *maximum a posteriori* (MAP) estimation by which the high-level configuration that has the overall maximum probability, given the

observation g, is obtained. A second possible criterion is to maximize the a posteriori marginal probability at each pixel, that is, obtain a classification of each individual pixel that has maximum probability, given the observation g, i.e. pixel-based segmentation.

The MAP segmentation involves the determination of $\hat{g}^h$ that maximizes $P(G^h = g^h|G = g)$ with respect to g^h. To illustrate the potential of the proposed color representation, we will consider two different color classification methods [11].

A. Parametric and non-parametric Bayes classification

In Bayes rule of Eq.(18), because the dominator does not affect the optimization, the MAP segmentation can be obtained, equivalently, by maximizing the numerator, that is, we need to find $\hat{g}^h$ that maximizes the numerator. The first term of the numerator is the likelihood due to the region information, and the second term is due to the high-level process. Thus, color classification of a pixel s can be rewritten as shown in Eq.(19).

$$P(G^h = g^h|G = g) = \frac{P(G = g|G^h = g^h)P(G^h = g^h)}{P(G = g)} \tag{18}$$

$$g^h(s) = k \quad if P(G^h = k|G = g) > P(G^h = i|G = g) \forall i \neq k \tag{19}$$

Two major values should be known for the classification process. The first one is the a priori probability for each color class, $P(G^h = g^h)$. The a priori probabilities can be estimated from the training dataset or, simply, they can be assumed to be equal. The second probability value that should be known is the conditional probability, $P(G = g|G^h = g^h)$. It can be estimated using one of two main schemes: parametric and non-parametric schemes. In the parametric schemes, the general form of the conditional density is known and the parameters in this form are to be estimated. For instance, considering a multi-dimensional Gaussian distribution, the mean vector and the covariance matrix are the needed parameters for estimation. *Maximum Likelihood Estimator (MLE)* is one of the most common approaches in the parametric estimation [11].

In the non-parametric approaches, the conditional density form does not have to be assumed. Parzen window [15] is a well-known non-parametric estimator. In this approach, the conditional density is estimated by counting the number of samples (K_n) from the training set that fall in a hypercube of volume (V_n), as shown in Eq.(20).

$$K_n = \sum_{i=1}^{n} \varphi(\frac{s - s_i}{h_n}) \tag{20a}$$

$$p(s|k) = \frac{K_n/V_n}{n} \tag{20b}$$

where n is the size of the training set and $\varphi(.)$ is the windowing function.

B. ICM algorithm

Point-based classification could cause many segmentation errors. Therefore, *Iterated Conditional Modes (ICM)* is used as a relaxation algorithm to find a local maximum [16]. The a posteriori probability of each pixel is estimated with the assumption that the classes for its neighbors are known. The high level process is assumed to be consisted of C independent processes. The first order Gibbs-Markov random field can be used to model each of these C processes [17], as shown in Eq.(21),

$$P(G^h = k|b) = \frac{1}{Z} e^{-\lambda m} \tag{21}$$

where b is the neighbor set, m is the neighborhood portion belonging to class k, Z is a normalization factor and can be neglected in comparing probabilities, and $\lambda$is the clique potential and usually takes a negative value. The larger values of $|\lambda|$ mean strong dependence on the neighbors and hence more homogeneity in the classification results. Several approaches have been developed to estimate this clique potential [11]. In this paper, we use Baye's for initial classification. Then, ICM is executed iteratively. Our stopping criterion is: the change in the pixels' assigned-classes should fall below a particular threshold.

V. Experimental Results

In this section, we prove, experimentally, the power of the proposed ECB versus the other color models as a robust and distinctive representation for colors in real images. We evaluate the performance of ECB as well as the classical models using the performance evaluation criteria described in section three, (*RD*) and (*SS*) measures. Forty-four segmented images from the flowers dataset of the COREL color image database are used as the training data to define the ECB transformation. We use the flowers dataset because the colors in these images have large perceptual variations, which represent a challenge to color segmentation algorithms. First, the integrated color descriptor of Eq.(7) is constructed using the nine primaries of NRGB, HSV, and YUV. Then, the ECB color descriptors are obtained by solving Eq.(12) for $\mathbf{W}$ and substituting in Eq.(9). The used three color models in the integrated descriptor are a mix between linear and nonlinear transformations of RGB space. In ECB, although $\mathbf{W}$ is a linear transformation of the integrated descriptor, it is nonlinear transformation of RGB space.

To evaluate RD of the ECB, the ratio between the intraset and interset distances are calculated for RGB, NRGB, HSV, YUV, XYZ, CIE-Lab, Ohta and ECB at different dimensions. Table (I(a)) shows the RD measures for the classical models. Table (I(b)) shows the RD measures for ECB as well as the percentage of error or information loss from the integrated vector due to the dimension reduction. From these two tables, it is clear that ECB with a dimension of three primaries is the best choice, since it preserves 98.27% from the color information of the integrated descriptor, and at the same time it has a better RD than the classical models.

TABLE I

RD MEASURE

(a) Classical color models

Model	RGB	NRGB	HSV	YUV	XYZ	LAB	Ohta	Integrated
RD	0.849	1.572	1.356	1.440	0.958	1.521	1.242	1.097

(b) ECB at different dimensions

Dimension	1	2	3	4	5
RD	2.717	1.775	1.584	1.529	1.519
Loss(%)	23.2	9.48	1.73	0.19	$9.7E^{-1}$
Dimension	6	7	8	9	
RD	1.519	1.519	1.519	1.519	
Loss(%)	$5.5E^{-1}$	$4.7E^{-1}$	$4.5E^{-1}$	0	

TABLE II

SS MEASURE

Model		ECB	RGB	NRGB	HSV	YUV	XYZ	LAB	Ohta
Bayes Classifier	Specificity (%)	85.33	79.21	65.70	90.2	79.22	79.04	80.88	78.88
	Sensitivity (%)	76.49	78.88	92.53	61.23	78.69	78.91	78.72	78.76
	SS (%)	80.79	79.04	77.97	74.32	78.95	78.98	79.79	78.82
ICM	Specificity (%)	87.73	81.86	67.49	91.83	81.84	81.61	83.16	81.40
	Sensitivity (%)	77.24	80.20	96.36	57.27	80.10	80.90	80.51	80.72
	SS(%)	82.14	81.03	80.64	72.52	80.97	81.25	81.82	81.06

To evaluate the performance of ECB in color segmentation, we consider the problem of segmenting colors in different real images based on both ECB and the classical models. For illustration purposes, we consider only three color classes for segmentation: green, yellow and red. For each model, the maximum likelihood estimator is used to estimate the densities for the three colors using pixels' colors in the training dataset. Then, parametric Baye's classifier is used for segmentation assuming Gaussian distribution for the colors. Also, ICM classifier is used with parametric Baye's classifier as an initialization. For qualitative comparison, Fig. 1 and 2 show sample segmentation results for Baye's and ICM classifiers. For quantitative comparison, Table (II) shows the SS measure for each model. Although, HSV gives the highest specificity values for both classifiers, it has the worst sensitivity values. Similarly, NRGB has the best sensitivity values and the worst specificity values. ECB has the best SS measure. Moreover, it has the second best sensitivity and specificity values for all classifiers. Fig. 3 shows qualitative results for segmenting a synthetic scene using Baye's classifier based on ECB as well as the classical color models. Although the colors in the scene are constructed synthetically and they are not exactly as natural colors like those in the training set, ECB gives the best segmentation results.

VI. CONCLUSION

In this paper, we presented the Eigen Color Basis (ECB) as a novel color representation for distinctive color segmentation. ECB is proposed as a more distinctive and robust color representation than the classical color models. Color segmentation using Baye's classifier and ICM has been used to evaluate the performance of ECB with respect to the classical models. The segmentation results have supported the high performance of ECB in distinctive color representation.

REFERENCES

[1] G. Wyszecki and W. S. Stiles. *Color Science: Concepts and Methods, Quantitative Data and Formulae*. John Wiley & sons, second edition, 1982.

[2] Ido Omer and Michael Werman. Color lines: Image specific color representation. In *Proceedings of the IEEE Conference on Computer Vision and Pattern Recognition (CVPR 04)*, volume II, pages 946–953. IEEE, June 2004.

[3] N. Vandenbroucke, L. Macaire, and J.G. Postaire. Color pixels classification in an hybrid color space. In *Proceedings of the IEEE International Conference on Image Processing - ICIP'98*, volume 1, pages 176–180, Chicago, 1998.

[4] N. Vandenbroucke, L. Macaire, and J. G. Postaire. Color image segmentation by pixel classification in an adapted hybrid color space: application to soccer image analysis. *Computer Vision and Image Understanding*, 90(2):190–216, 2003.

[5] J. M. Tenenbaum, T. D. Garvey, S.Weyl, and H. C.Wolf. An interactive facility for scene analysis research. Technical Report 87, Artificial Intelligent Center, Stanford Research Institute, Menlo Park, CA, 1974.

[6] A. R. Smith. Color gamut transform pairs. In *SIGGRAPH '78: Proceedings of the 5th annual conference on Computer graphics and interactive techniques*, pages 12–19, New York, NY, USA, 1978. ACM Press.

[7] K. Plataniotis and A. Venetsanopoulos. *Color Image Processing and Applications*. Springer Ed., 2000.

[8] H. Palus. Colour spaces. In S.J. Sangwine and R.E.N. Horne, editors, *The Colour Image Processing Handbook*, pages 67–90. Chapman & Hall, Cambridge, Great Britain, 1998.

[9] http://www.cie.co.at/cie/index.html.

[10] Y. I. Ohta, T. Kanade, and T. Sakai. Color information for region segmentation. *Computer Graphics and Image Processing*, 13:222–241, 1980.

[11] R. O. Duda, P. E. Hart, and D. G. Stork. *Pattern Classification*. Wiley-Interscience Publication, second edition, 2000.

(a) Original image

(b) Ground truth

(c) ECB

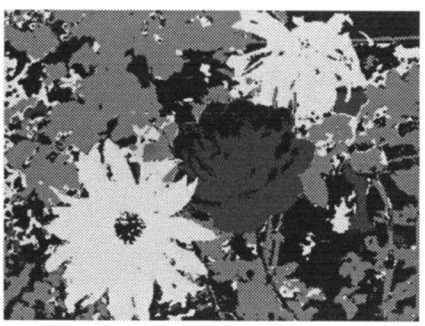

(d) RGB

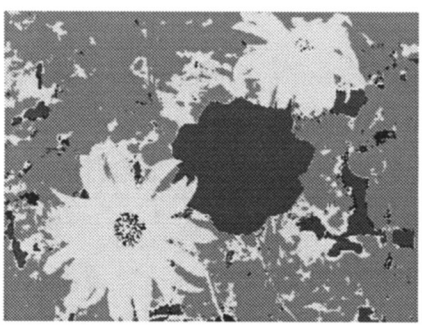

(e) NRGB

(f) HSV

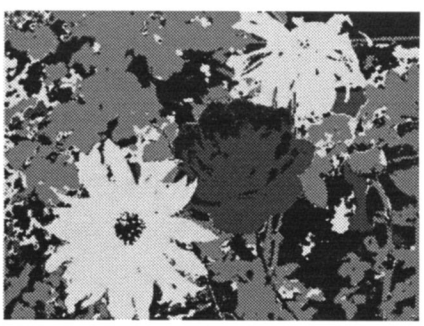

(g) YUV

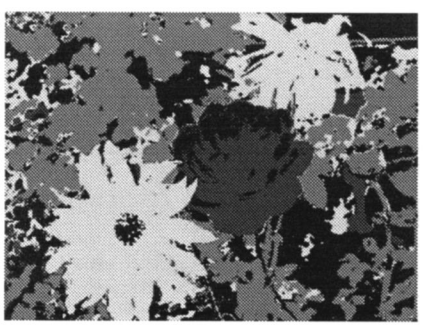

(h) Ohta

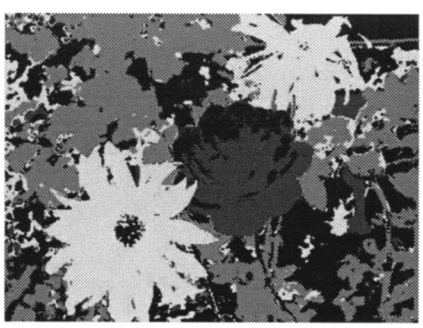

(i) XYZ

(j) LAB

Fig. 1. Segmentation results using Baye's classifier

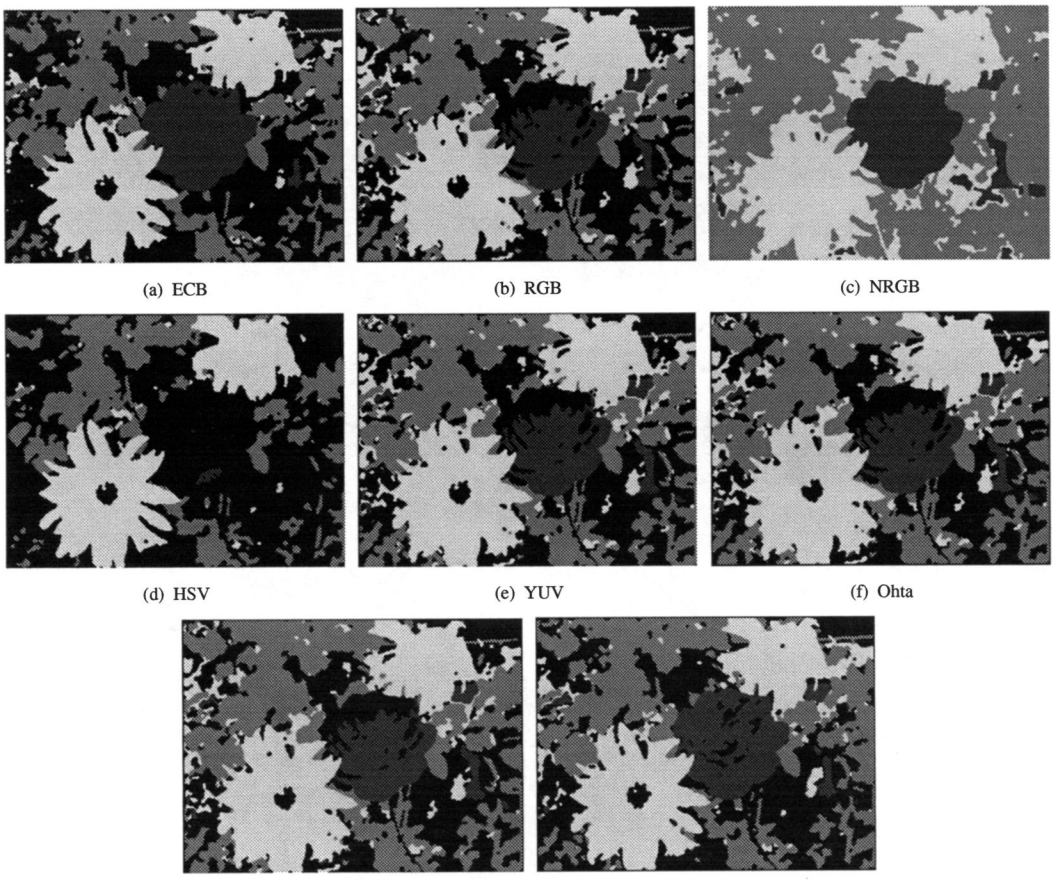

(a) ECB (b) RGB (c) NRGB

(d) HSV (e) YUV (f) Ohta

(g) XYZ (h) LAB

Fig. 2. Segmentation results using ICM algorithm

[12] E. Littmann and H. Ritter. Adaptive color segmentation—a comparison of neural and statistical methods. *IEEE Transactions on Neural Networks*, 8(1):175–185, January 1997.

[13] J. Gauch. Segmentation and edge detection. In S.J. Sangwine and R.E.N. Horne, editors, *The Colour Image Processing Handbook*, pages 163–187. Chapman & Hall, Cambridge, Great Britain, 1998.

[14] A. Farag and E. Delp. Image segmentation based on composite random field models. *Optical Engineering*, 12:2594–2607, December 1992.

[15] E. Parzen. On the estimation of a probability density function and the mode. *Annals of Mathematical Statistics*, 33:1065–1076, 1962.

[16] J. Besag. On the statistical analysis of dirty pictures. *Journal of the Royal Statistical Society*, B-48:259–302, 1986.

[17] A. Farag, R. Mohamed, and H. Mahdi. Experiments in image classification and data fusion. In *5th International Conference on Information Fusion*, volume 1, pages 299–308, Annapolis, MD, July 2002.

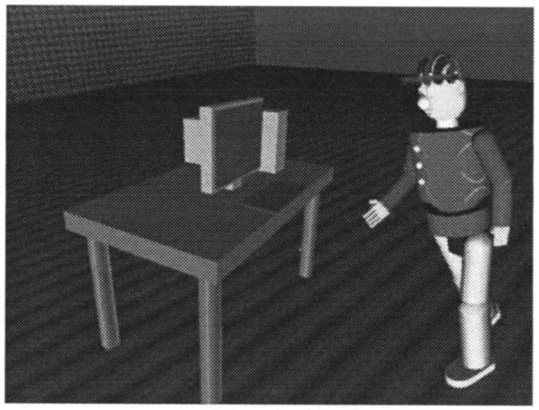

(a) Original image

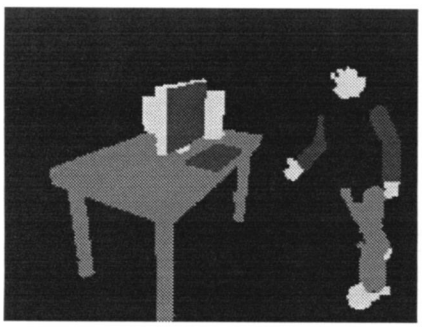

(b) Ground truth

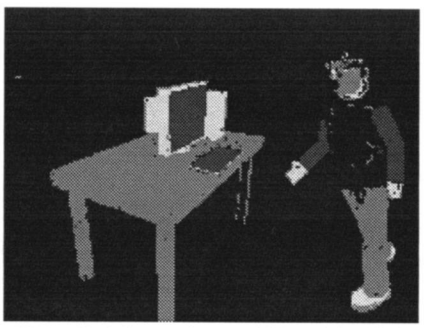

(c) ECB

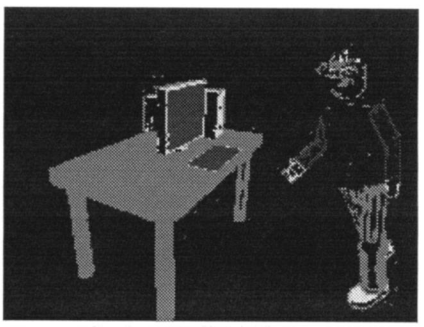

(d) RGB

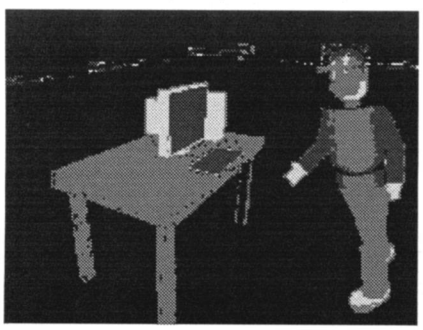

(e) NRGB

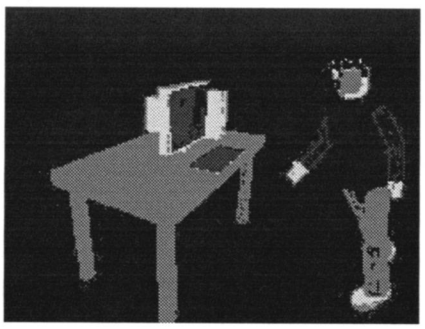

(f) HSV

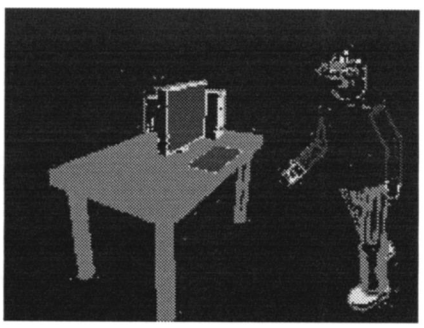

(g) YUV

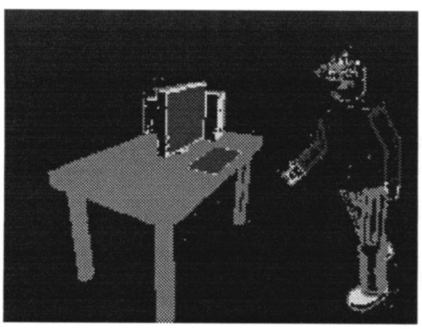

(h) Ohta

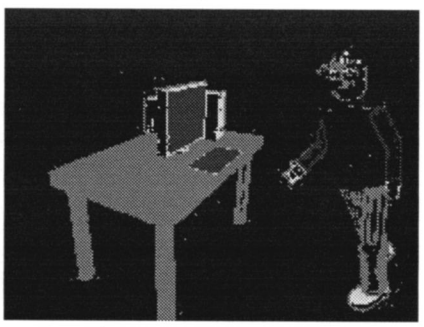

(i) XYZ

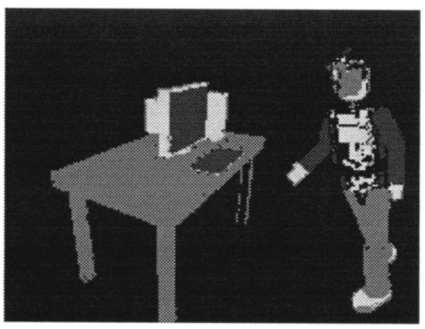

(j) LAB

Fig. 3. Segmentation results using Baye's classifier